Monthly Notices
of the
ROYAL ASTRONOMICAL SOCIETY

Mon. Not. R. Astron. Soc. **403,** 906–919 (2010) doi:10.1111/j.1365-2966.2009.16169.x

Quasars probing intermediate-redshift star-forming galaxies

P. Noterdaeme,⋆ R. Srianand⋆ and V. Mohan⋆

Inter-University Centre for Astronomy and Astrophysics, Post Bag 4, Ganeshkhind, 411 007 Pune, India

Accepted 2009 December 4. Received 2009 December 3; in original form 2009 September 17

ABSTRACT

We present a sample of 46 [O III]-emitting galaxies at $z < 0.8$ detected in the fibre spectra of quasars from the Sloan Digital Sky Survey, Data Release 7 (SDSS-DR7) through an automatic search procedure. We also detect [O II] and Hβ emission lines from most of these galaxies in the SDSS spectra. We study both the emission and absorption properties of a subsample of 17 galaxies in the redshift range $z = 0.4$–0.7, where Mg II lines are covered by the SDSS spectra. The measured lower limits on the star formation rates of these galaxies are in the range 0.2–20 $M_\odot$ yr^{-1}. The emission-line luminosities and (O/H) metallicities from R23 measured in this sample are similar to what is found in normal galaxies at these redshifts. Thus, this constitutes a unique sample of intermediate-redshift star-forming galaxies where we can study the quasi-stellar object (QSO) absorber–galaxy connection. Strong Mg II ($W_{\lambda2796} \gtrsim 1$ Å) as well as Mg I absorption lines are detected in the QSO spectra at the redshift of most of these galaxies. Strong Fe II ($W_{\lambda2600} > 1$ Å) absorption lines are also generally detected whenever the appropriate wavelength ranges are covered. This suggests that most of these systems could be bona fide damped Lyman α systems. We investigate various possible relations between the Mg II rest equivalent widths and the emission-line properties. We find a possible (2σ) correlation between the emission-line metallicity of the galaxies and the Mg II rest equivalent width of the absorbers [$\log(\mathrm{O/H}) + 12 = 0.1 W_{\lambda2796} + 8.27$], which could be a consequence of an underlying mass–metallicity relation. However, [O III]-selected Mg II systems represent only a minor fraction of the strong Mg II absorbers. We find this cannot be attributed to biases related either to the spectral signal-to-noise ratio or to the brightness of the QSOs. We measure the average observed fluxes (collected into the SDSS fibre) of the [O II] and [O III] lines associated to Mg II-selected systems through stacking technique. We find that the average luminosities of emission lines are higher for systems with larger $W_{\lambda2796}$. The stacked luminosities are found to be below the typical detection limit in individual spectra, indicating that faint galaxies can contribute appreciably to the observed population of strong Mg II absorbers at intermediate redshifts. We also present long-slit spectroscopic observations of SDSS J113108+202151, the most luminous line-emitting galaxy in our $z \geq 0.4$ sample. Surprisingly, we find that the line-emitting region does not coincide with the nearby extended bright galaxy with consistent photometric redshift seen in the SDSS image.

Key words: galaxies: abundances – galaxies: fundamental parameters – galaxies: ISM – quasar: absorption lines – quasar: individual: SDSS J113108+202151.

1 INTRODUCTION

The study of intervening absorption lines seen in the spectra of bright distant objects is one of the most sensitive and powerful probes for understanding the early evolution of galaxies. Indeed, at low and intermediate redshifts ($z \lesssim 1$), the connections between quasi-stellar object (QSO) absorption systems and galaxies are mainly investigated for Mg II-selected systems. These absorbers are found to be statistically associated with relatively bright field galaxies seen within a few tens of kpc to the QSO line of sight (Bergeron & Boissé 1991; Steidel 1995). These studies established that Mg II absorbers provide an unbiased way to detect normal galaxies at different redshifts. However, the success rate of detecting Mg II absorption in the spectrum of QSOs that have known foreground galaxies with redshift measurements is much less than one (Bechtold & Ellingson 1992; Bowen, Blades & Pettini 1995; Tripp

⋆E-mail: pasquiern@iucaa.ernet.in (PN); anand@iucaa.ernet.in (RS); vmohan@iucaa.ernet.in (VM)

& Bowen 2005). These studies suggest that the gaseous haloes around galaxies may be less uniformly populated than what was thought before (see Kacprzak et al. 2008). Also it is not necessary that the galaxies responsible for Mg II absorption are always bright $L_\star$ galaxies.

Integral field spectroscopy seems to be a promising technique for the study of galaxies associated to quasar absorption line systems and allowed Bouché et al. (2007) to detect Hα emission associated to 14 strong $z \sim 1$ Mg II absorbers (with impact parameters in the range 1–40 kpc), indicating large star formation rates (SFRs) (1–20 $M_\odot$ yr^{-1}). Another possibility is to directly search for galaxy light from Mg II absorbers in special cases where the quasar flux at short wavelengths is switched off by a higher redshift Lyman-limit system (Christensen et al. 2009). Till now, such observations have only resulted in stringent upper limits on the broad-band luminosity of the related galaxies.

It has also been proposed that other classes of QSO absorbers, such as those characterized by strong Ca II absorption lines, could select the most metal-rich gas (see e.g. Wild, Hewett & Pettini 2006; Nestor et al. 2008), hence probing more central parts of high-redshift galaxies. Wild, Hewett & Pettini (2007) have statistically detected [O II] emission associated to strong Mg II- and Ca II-selected absorbers by stacking Sloan Digital Sky Survey (SDSS) quasar spectra. However, only a few direct detections of emission lines from absorbing galaxies have been reported so far. Zych et al. (2007) presented direct imaging and long-slit spectroscopic observations of five quasars with strong Ca II systems at $z < 0.5$. They detected [O II], [O III], Hα and Hβ emission lines at the redshift of the absorbers. The luminosity of the corresponding galaxies is high, $L \simeq L_\star$, with SFRs in the range 0.3–30 $M_\odot$ yr^{-1}.

When galaxies are detected with some projected separation to the QSO sightline it is not obvious whether one is detecting the halo gas associated with the galaxy or one is probing the correlation length of metals in the intergalactic medium with respect to the bright galaxies. The contribution of possible faint galaxies closer to the line of sight (i.e. within the point spread function of the QSO) that remain undetected is also not well explored. Therefore, even after two decades of intense research activity to establish the Mg II absorber–galaxy relationship, there are still open questions in this field that need to be answered.

Here, we present direct detections of emission lines from intervening star-forming galaxies (with impact parameters $\leq$10 kpc and redshifts in the range $0.1 \leq z \leq 0.8$) in quasar spectra from the Sloan Digital Sky Survey Data Release 7 (SDSS-DR7). For objects at $z \geq 0.4$, the SDSS spectra allow us to search for Mg II absorption originating from these galaxies. Our approach is very different from all previous ones in the sense that we do not make any pre-selection of galaxies based on QSO absorption lines. On the contrary, we take advantage of SDSS fibre spectra, by first searching for galaxy emission lines on top of background quasars spectra, then looking for the associated absorption lines. Throughout the paper, we adopt a Λ cold dark matter cosmology with $\Omega_{\rm m} = 0.3$, $\Omega_\Lambda = 0.7$ and $H_0 = 70\,{\rm km\,s^{-1}\,Mpc^{-1}}$ (e.g. Spergel et al. 2003).

2 SEARCH FOR INTERVENING GALAXIES

We are mostly interested in detecting normal star-forming galaxies close to the line of sight of background QSOs. We focus on the redshift range $z = 0.4$–0.7 as most prominent emission lines, as well as the Mg II absorption lines, fall in the spectral range covered in the SDSS spectrum. In particular, [O III] doublet lines are useful because the [O III]λ5007 is one of the strongest lines in the optical range and is accompanied by the close-by [O III] λ4959 line with a fixed intensity ratio, allowing for an easy identification using an automated procedure. In this section, we derive a rough estimate of the expected number of [O III] emitters that can be detected from the SDSS QSO spectra, describe our automatic routine to detect galaxies and discuss the bias due to QSO luminosity.

2.1 Detectability and number density of faint galaxies

Here we try to get a rough estimate of the number of galaxies with different [O III] luminosities at $0.4 \leq z_{\rm gal} \leq 0.8$ that will be within the SDSS fibre centred around a distant QSO. The expected peak flux of the [O III]λ5007 emission from a $L^\star_{[{\rm O\,III}]}$ galaxy [$\log L^\star_{[{\rm O\,III}]}$ (erg s^{-1}) = 41.95; Hippelein et al. 2003] at $z = 0.5$ will be of the order of $F_\star(z = 0.5) \sim 10^{-16}\,{\rm erg\,s^{-1}\,cm^{-2}\,\AA^{-1}}$, assuming a linewidth full width at half-maximum (FWHM) $\simeq 5$ Å. Note that, throughout the paper, $L^\star_{[{\rm O\,III}]}$ refers to the Schechter parameter of the [O III] luminosity function. As we aim here at detecting low-luminosity galaxies, we should reach a detection limit of the order of $10^{-17}\,{\rm erg\,s^{-1}\,cm^{-2}\,\AA^{-1}}$.

If we assume the dominant noise for the detection of an emission line is the photon noise from the quasar continuum (i.e. we ignore the background noise), then the signal-to-noise ratio (S/N) in the peak of the emission line, S/N_l, can be written as

$$S/N_l = \frac{N_l}{\sqrt{(N_c + N_l)}}, \quad (1)$$

where N_l and N_c are the counts in the line and in the continuum, respectively. The S/N of the continuum, S/N_c, is equal to $N_c/\sqrt{N_c}$ and the count ratio is equal to the flux ratio ($N_l/N_c = F_l/F_c$). Therefore, we can write

$$S/N_l = S/N_c \frac{F_l/F_c}{\sqrt{1 + F_l/F_c}}. \quad (2)$$

The detectability of the emission line will not only depend on the [O III] line flux (F_l) but also on the quasar flux (F_c). For a given emission-line flux, the minimum S/N required to detect the [O III] emission will depend upon the magnitude of the quasar. That is, the 3σ detection of the [O III]λ5007 emission line arising from an $L_0 = 0.2L^\star_{[{\rm O\,III}]}$ galaxy towards an $i = 19$ quasar will require a spectrum with S/N $\geq$10. In turn, detecting the same galaxy towards an $i = 17$ quasar will require a S/N higher than about 45.

Next, we estimate the probability of a given line of sight to pass very close or through a galaxy with line luminosity greater than a limiting luminosity L_0. Integrating the [O III] luminosity function over the luminosities gives the number density of galaxies:

$$n_{L>L_0} = \int_{L_0}^{\infty} \Phi(L)\,{\rm d}L = \Phi_\star \Gamma\left(\alpha + 1, \frac{L_0}{L^\star_{[{\rm O\,III}]}}\right), \quad (3)$$

where $\Phi_\star, \alpha$ and $L^\star_{[{\rm O\,III}]}$ are the Schechter parameters of the luminosity function, taken from table 5 of Ly et al. (2007) and $\Gamma(a, b)$ is the incomplete gamma function. We can estimate the number of galaxies with an impact parameter less than the SDSS fibre radius (1.5 arcsec, i.e. $r \sim 10$ kpc at $z \sim 0.5$):

$$N_{L>L_0} = \pi r^2 n_{L>L_0}. \quad (4)$$

For $L_0 = 0.2L^\star_{[{\rm O\,III}]}$, this gives us a number density per unit distance $N_{L>0.2L\star} \sim 1$–$2 \times 10^{-6}\,{\rm Mpc^{-1}}$. That is, for a line of sight to a quasar probing $z \sim 0.4$–0.6, the probability of an $L \geq 0.2L^\star_{[{\rm O\,III}]}$ galaxy being at an impact parameter less than the SDSS fibre radius will be about 5–10×10^{-4}. We need to consider this as a very conservative upper limit as while estimating this number we have not considered

(1) any bias due to the luminosity of the background QSO (see Section 2.3), (2) the emission-line attenuation due to dust internal to the galaxy, (3) the fibre losses (i.e. the fact that only a fraction of [O III] flux may go through the fibre) and (4) the colour selection of QSOs missing dusty sightlines (Noterdaeme et al. 2009a), as expected from galaxies at very low-impact parameters. From these simple-minded calculations, one can already see that a huge number of quasar spectra ($>10^4$) with adequate S/N will be required to detect a handful of star-forming galaxies with an impact parameter $\leq$10 kpc along the line of sight to distant QSOs. The availability of a large number of high-quality QSO spectra in the SDSS data base makes it a realistic possibility to build a sample of such star-forming galaxies to bridge the connection between strong Mg II systems and star-forming galaxies.

2.2 Search for galaxy [O III] lines in SDSS quasar spectra

We employ a correlation analysis to select emission-line galaxies close to the line of sight to 98 978 quasars from the SDSS II DR7, without any prior knowledge of the absorption properties of the galaxies. As a first step, we iteratively fit the quasar continuum by applying Savitsky–Golay filtering and removing deviant pixels. We then cross-correlate the continuum-subtracted quasar spectra with a template profile of [O III]$\lambda\lambda$4959, 5007 generated from the SDSS galaxy template spectrum.

We restrict our search out of the Lyman α forest (in particular for high-redshift QSOs) and below $\lambda = 8400$ Å (i.e. $z_{\rm gal} < 0.68$) to avoid the most crowded telluric line regions. Whenever a high correlation is found ($C > 0.9$), we check the [O III]λ5007 (respectively [O III]λ4959) are detected at more than 2σ (respectively 1σ) level. Note that because of the galactic template used, wide emission lines arising from active galactic nuclei are not picked up by our procedure. Each candidate was then inspected visually for the presence of other emission lines, in particular Hβ, Hγ and [O II]$\lambda\lambda$3726, 3729. Spurious detections were identified and removed from the sample. We list all the 44 confirmed emission-line galaxies in the redshift range $0.1 \leq z_{\rm gal} \leq 0.68$ in Table 1. 17 of these galaxies are in the redshift range ideally suited for detecting Mg II absorption in the SDSS spectrum itself. These objects form the main sample of this present study.

In addition, we performed an automatic search for the [O II]$\lambda\lambda$3726, 3729 emission doublet[1] associated to Mg II systems to detect higher redshifts systems, for which telluric lines make any search based on [O III] a difficult task. Mg II systems were found by an automatic procedure based on correlation analysis, similar to that used by Noterdaeme et al. (2009b) to search for damped Lyman-α systems (DLAs). This provided us with two additional galaxies, at $z = 0.669$ and 0.788 towards SDSS J120908+022734 and SDSS J161728+061604, respectively. The detections are summarized in Table 1. We concentrate, in this paper, on the sample of 17 [O III]-selected galaxies at $0.4 < z_{\rm gal} < 0.7$ for which the expected positions of the Mg II $\lambda\lambda$2796, 2803 absorption lines are also covered. Lower redshift systems are also provided in Table 1 for the interested reader.

2.3 Effect of QSO luminosity

In Fig. 1, we present the fibre magnitudes and spectral S/N in *i* band of the whole quasar sample searched for [O III] emission lines and compare to that of quasars with detected intervening emission lines.

[1] The two lines are always blended at the SDSS resolution.

Table 1. Sample of galaxies with [O III] emission around QSO sightline.

QSO	Plate, MJD, fiber	$z_{\rm QSO}$	$z_{\rm gal}$[a]	Selection
J023914–070557	0455, 51909, 562	0.715	0.342	[O III]
J080216+143506	2266, 53679, 154	1.562	0.141	[O III]
J080808+064108	1756, 53080, 184	2.108	**0.433**	[O III]
J081154+202148	1925, 53327, 437	1.247	**0.445**	[O III]
J082057+400326	0760, 52264, 075	0.588	0.301	[O III]
J085113+071959	1299, 52972, 256	1.654	0.130	[O III]
J091417+325955	1592, 52990, 275	4.656	**0.444**	[O III]
J092913+302225	1939, 53389, 537	1.815	**0.439**	[O III]
J094041+341535	1594, 52992, 048	1.718	**0.447**	[O III]
J094335-004322	0266, 51630, 125	0.271	0.099	[O III]
J094759+120537	1742, 53053, 624	1.287	0.257	[O III]
J095228+032616	0571,52286,144	1.290	**0.419**	[O III]
J101246+171419	2587, 54138, 556	1.103	0.112	[O III]
J103309+205956	2376, 53770, 427	1.113	0.361	[O III]
J104223+092708	1240, 52734, 584	1.108	**0.592**	[O III]
J104257+074850	1000, 52643, 522	2.666	0.033	[O III]
J110224+573512	0950, 52378, 241	1.620	0.293	[O III]
J111343+184002	2490, 54179, 023	2.062	0.169	[O III]
J112146+021757	0511, 52636, 175	1.274	0.263	[O III]
J113002+602628	0952, 52409, 403	0.374	0.061	[O III]
J113108+202151	2502, 54180, 371	1.763	**0.563**	[O III]
J114340+520303	0881, 52368, 313	1.816	0.132	[O III]
J120538+604057	0954, 52405, 535	0.537	**0.434**	[O III]
J120908+022734	0517, 52024, 541	1.226	**0.669**	Mg II+[O II]
J121510+141802	1765, 53466, 068	1.299	**0.421**	[O III]
J122752+165522	2598, 54232, 188	3.348	**0.565**	[O III]
J125339+175832	2601, 54144, 625	0.505	**0.401**	[O III]
J131804+522510	1667, 53430, 420	2.990	0.393	[O III]
J132542+255525	2244, 53795, 141	1.439	**0.433**	[O III]
J133733+445129	1465, 53082, 300	1.168	0.159	[O III]
J132918+630424	0603, 52056, 089	0.987	0.366	[O III]
J140103-005030	0301, 51942, 052	0.927	0.357	[O III]
J140159+414156	1346, 52822, 060	1.701	0.120	[O III]
J142421+453523	1287, 52728, 101	1.614	**0.421**	[O III]
J143458+504118	1046, 52460, 542	1.485	0.199	[O III]
J144412+022301	0536, 52024, 626	1.215	0.140	[O III]
J145240+544345	1163, 52669, 505	1.520	0.102	[O III]
J150140+571026	0610, 52056, 133	1.799	0.103	[O III]
J154542+505759	0796, 52401, 495	0.942	**0.525**	[O III]
J160521+510740	0620, 52375, 535	1.229	0.099	[O III]
J161016+500728	0623, 52051, 304	0.239	0.127	[O III]
J161607+212401	1853, 53566, 192	1.115	0.335	[O III]
J161728+061604	1731, 53884, 113	1.244	**0.788**	Mg II+[O II]
J165508+224150	1415, 52885, 478	0.621	**0.453**	[O III]
J165632+414617	0631, 52079, 118	2.163	**0.662**	[O III]
J235621+002906	0387, 51791, 343	1.049	0.331	[O III]

[a]The redshifts of galaxies studied in this paper, $z_{\rm gal} \geq 0.4$, are marked in bold face.

It is somehow surprising to see that the detections do not occupy any preferred region of the S/N–magnitude diagram. This is better seen in the upper (respectively right) panel where we compare the differential and cumulative distributions of the magnitudes (respectively S/N) of QSOs with and without a foreground [O III]-emitting galaxy. Indeed, a double-side Kolmogorov–Smirnov (KS) test shows that the probability of the magnitudes of the quasar with [O III]-selected intervening galaxies to arise from the same parent population as the whole quasar sample is high ($P_{\rm KS} = 0.88$). The same test on S/N gives $P_{\rm KS} = 0.60$.

Following equation 2, we overplot the S/N required for the 1σ detection of an emission line with peak intensity $F_{\rm l} = 10^{-17}$ erg s^{-1} cm^{-2} Å^{-1} (or equivalently the 3σ detection of

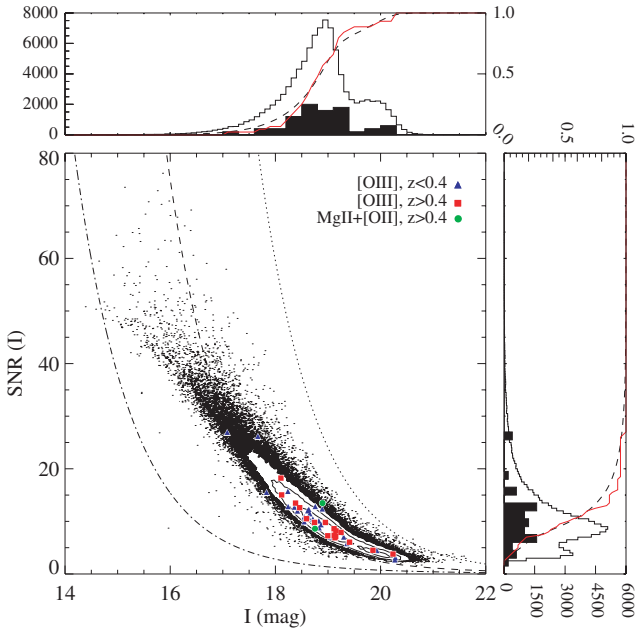

Figure 1. *i*-band S/N and magnitude of the searched quasars. Contours are drawn in the region with highest density of points for presentation purpose. The upper and right-hand panels show, respectively, the magnitude and the S/N distributions for the whole quasar sample (unfilled histogram) and for quasars selected upon the presence of intervening [O III] emission line (filled histogram). The filled histograms have been scaled for presentation purpose only. Dotted (respectively solid) curves on the top and right-hand panels represent the normalized cumulative distributions for the whole quasar sample (respectively quasars with [O III]-selected intervening galaxies). The three curves in the main panel represent the minimum S/N required for the 1σ detection of a emission line with peak flux $F_l = 1/5 \times 10^{-17}$ (dotted), 10^{-17} (dashed) and 5×10^{-17} (dashed–dotted) erg s^{-1} cm^{-2} Å^{-1}.

$F_l = 3 \times 10^{-17}$ erg s^{-1} cm^{-2} Å^{-1}) as a function of the *i*-band magnitude of the background quasar. The spectral S/N and *i*-band magnitudes of the quasars roughly follow this relation. While detections are naturally made easy towards faint quasars, the steeply increasing S/N of SDSS spectra with the quasar brightness also allows for detections towards relatively bright quasars. However, the S/N reached by the SDSS for the very bright quasars ($i < 17$) are still not sufficiently high to detect intervening emission lines with $F_l \sim 10^{-17}$ erg s^{-1} cm^{-2} Å^{-1}. As can be seen in the top panel of Fig. 1, quasars with $i < 17$ are rare anyway and do not contribute much to the statistics.

3 EMISSION-LINE ANALYSIS

The [O II]λλ3726, 3729 doublet and Hβ are the other strong lines that are expected in the wavelength range covered by the SDSS spectrum for the redshift range of our interest. We detect [O II]λλ3726, 3729 in all the cases except for the $z = 0.445$ galaxy along the line of sight towards J081154+202148. However, it is obvious from Fig. 2 that the S/N in the wavelength range of [O II] emission is poor. The Hβ line is detected in all but two cases. Here we perform a detailed analysis of Hβ, [O III] and [O II] emission lines through Gaussian fitting. As a first step, we subtract the continuum emission that includes the continuum light from both the QSO and the galaxy. The unabsorbed continuum (including the quasar broad emission lines but excluding intervening emission lines) is determined accurately by manually adjusting a spline function to the observed spectrum. Then we simultaneously fit the detected emission lines using an IDL code based on MPFIT (Markwardt 2009), which performs χ^2-minimization by Levenberg–Marquardt technique. We use a single redshift for all emission lines. The [O II]λλ3726, 3729 doublet is fitted with a double Gaussian. Note that although the two lines are always blended at the SDSS spectral resolution, it is still possible to distinguish the two corresponding peaks. As the flux ratio of these two lines depends on the kinetic temperature of the gas and the electron density (e.g. Kisielius et al. 2009), we fit the blend with two components allowing for the relative flux ratio to be a free parameter but keeping the linewidths tied. In the case of the forbidden lines [O III]λλ4959, 5007, we impose the line ratio to follow the theoretical value of 3 (e.g. Storey & Zeippen 2000). The results of our fits are shown in Fig. 2. The integrated line intensities of [O III], [O II] and Hβ lines are then measured from the fitted Gaussian parameters. In the following, we always refer to [O III] flux (or luminosity) as the sum of fluxes (or luminosity) of [O III]λ5007 and [O III]λ4959. Similarly, in the case of [O II], we use the sum of [O II]λ3727 and [O II]λ3730. The total emission-line flux together with the associated errors are given in Table 2. In the case of non-detection, we give 2σ upper limits.

3.1 Luminosities

Using the measured redshifts and fluxes, we estimate the emission-line luminosities for the cosmological parameters noted above. Luminosities for all the three lines are also summarized in Table 2. Note that we do not apply any correction for the dust reddening or the fact that the fibre need not sample the whole galaxy. This means that the quoted luminosities should be treated as lower limits. In Fig. 3, we compare the distribution of the measured [O III] luminosities of our galaxies and the [O III] luminosity functions at $z = 0.4$–0.6 from Hippelein et al. (2003). The vertical dotted line marks the luminosity of a $L^\star_{[\mathrm{O\,III}]}$ galaxy. As expected, we mostly detect galaxies with luminosities in the range 0.1–3$L^\star_{[\mathrm{O\,III}]}$, with a median [O III] luminosity $L_{[\mathrm{O\,III}]} \sim 0.2L^\star_{[\mathrm{O\,III}]}$. The galaxy along the line of sight towards J113108+202151 has $L_{[\mathrm{O\,III}]} \sim 2L^\star_{[\mathrm{O\,III}]}$. We study this system in detail using our observations with IUCAA Girawali observatory (IGO) in Section 6.

The sharp decrease seen in the number of galaxies detected at the low-luminosity end ($\log L_{[\mathrm{O\,III}]} < 41$) is a consequence of our detectability limit, as can be seen from the departure from the dotted curve in Fig. 3, while the decrease at high luminosities ($\log L_{[\mathrm{O\,III}]} > 42$) is a natural consequence of the decrease in the number density of very luminous galaxies. As there is a factor of 30 spread in the luminosity, this set of galaxies provides a good sample for various followup studies such as measuring the cross-section and filling factor of Mg II absorbers at low-impact parameters (i.e. $\leq$10 kpc).

3.2 Star formation rates

In this section, we aim at deriving the SFRs of intervening galaxies using emission-line luminosities. It is known that the relationship between the observed luminosity of a line and SFR depends on dust extinction and metallicity (see for example Argence & Lamareille 2009). In the redshift range of galaxies that we focus on in this paper, the Hα line redshifts into the near-IR wavelengths. Thus, we cannot use the Balmer decrement to get the dust extinction. Also, as the continuum of the galaxy is combined with that of the QSO, we cannot use the spectral energy distribution (SED) fitting to get the estimates for reddening.

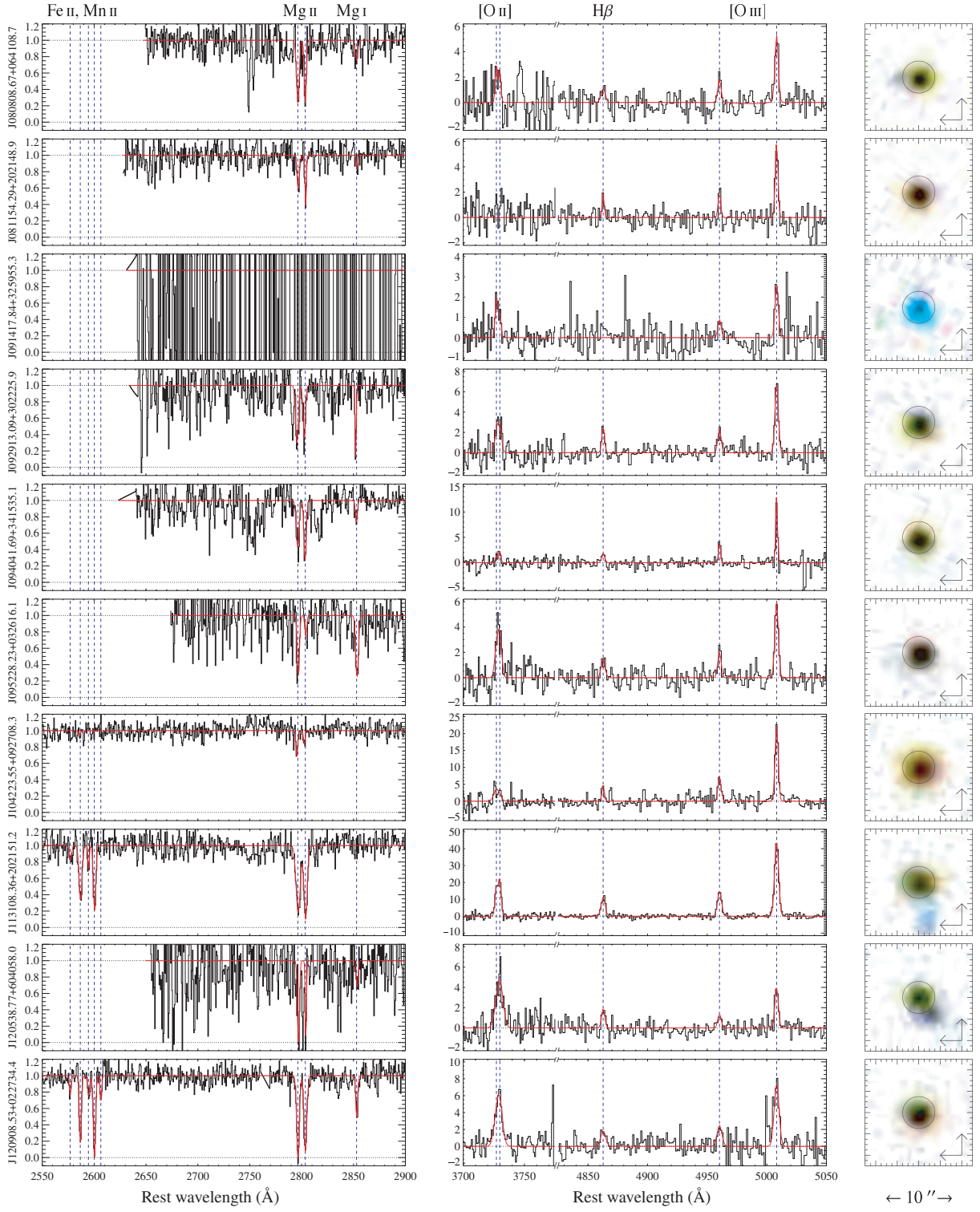

Figure 2. Absorption (left) and emission (middle) lines from the intervening galaxies. Note that in the left-hand panels (absorption), the spectrum is normalized by dividing the observed spectrum by the QSO continuum, while in the middle panels (emission), the QSO continuum is subtracted from the observed spectrum and the flux scale is in units of 10^{-17} erg s^{-1} Å^{-1}. Best-fitting absorption and emission lines are overplotted. The SDSS images of the QSOs are shown in the right-hand panels. The black circle represents the position of the 3-arcsec-diameter SDSS fibre. North is top and East is left.

Using more than 100 000 star-forming galaxies from SDSS, Argence & Lamareille (2009) have provided fitting formulae (their equations 23 and 24) that use uncorrected [O II] and [Hβ] luminosities to get the SFRs. The typical quoted dispersion in the SFR is about 0.23 dex. As noted by Argence & Lamareille (2009), the SFR derived using their equation (23) is weakly sensitive to the variations in dust attenuation. However, their equation (24) provides a SFR estimate that is weakly sensitive to the variations in metallicity.

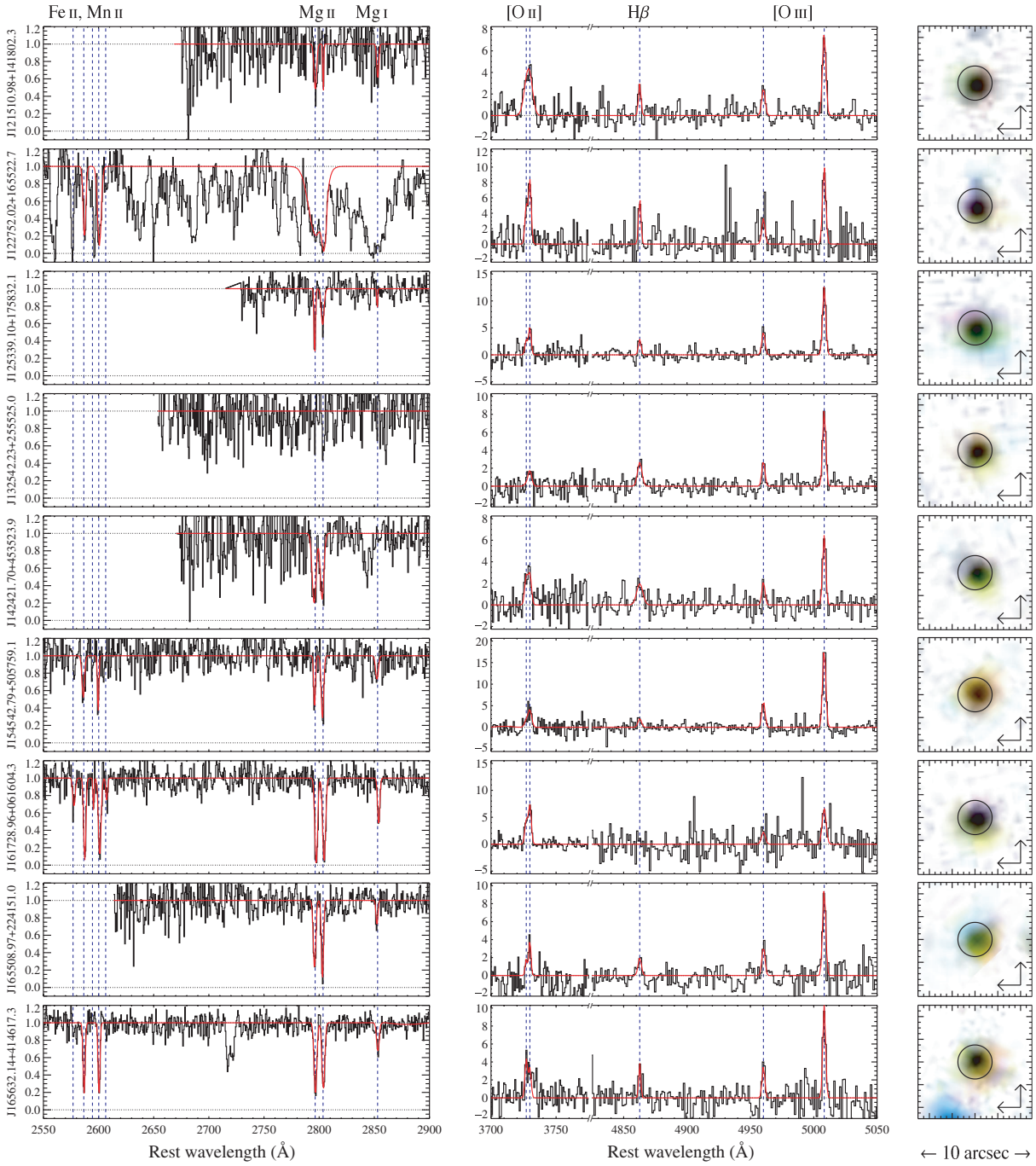

Figure 2 – *continued*

Thus, for each galaxy we consider the SFR estimates based on the above mentioned two equations to provide the realistic range in SFR (last column in Table 2). In this table, we also give SFR based only on the [O II] and [Hβ] calibrators. However, these estimates should be treated as lower limits as the SDSS fibres may collect only part of the emission from the galaxies.

It is clear from Table 2 that the SFR in the galaxies in our sample varies between 0.2 and 20 $M_\odot$ yr^{-1}. Roughly half of the galaxies in the sample have an SFR less than 2 $M_\odot$ yr^{-1}. Note that in the case of J132542+255525, there is a very large spread between the SFRs derived using the different calibrators. We caution that the [O II] and Hβ emission lines in this system are close to the detection limit and using their ratio may lead to a significant overestimation of the SFR and metallicities (see next section). It is interesting to note that all the five Ca II absorption selected galaxies studied by Zych et al. (2007) have an SFR similar to that of galaxies in our sample.

3.3 Emission-line metallicities

We use the R23 ratio, ([O II]+[O III])/Hβ, as calibrated by Kobulnicky, Kennicutt & Pizagno (1999) to measure the metallicities. This calibration provides two solutions for most values of R23, a low- and a high-metallicity estimates. These are generally referred to as 'lower' and 'upper' branches of R23. The use of additional

Table 2. Star formation rates of the intervening galaxies.[a]

QSO	z_{gal}	$F_\lambda(10^{-17}$ erg s^{-1} cm^{-2})			L (10^{40} erg s^{-1})[b]			SFR ($M_\odot$ yr^{-1})		
		[O II]	[O III]	Hβ	[O II]	[O III]	Hβ	[O II][c]	Hβ[c]	[O II]+Hβ[d]
J080808+064108	0.433	12.1(4.2)	25.1(3.0)	4.9(3.4)	8.3(2.9)	17.2(2.8)	6.7(4.7)	0.4	0.8	0.9
J081154+202148	0.445	$\leq$6	22.0(2.6)	4.0(1.8)	$\leq$4.2	16.1(2.5)	5.8(2.7)	–	0.7	–
J091417+325955	0.444	8.3(2.0)	12.3(1.9)	$\leq$5	6.0(1.4)	8.9(1.8)	$\leq$3.6	0.3	–	–
J092913+302225	0.439	16.9(8.2)	32.2(2.6)	7.4(2.3)	12.0(5.8)	22.8(2.4)	10.4(3.3)	0.5	1.2	1.7
J094041+341535	0.447	7.6(3.2)	33.7(4.2)	5.7(2.4)	5.6(2.3)	24.8(4.1)	8.4(3.6)	0.2	0.9	3.1–4.3
J095228+032616	0.419	21.1(7.4)	29.2(2.5)	6.1(3.2)	13.4(4.7)	18.5(2.1)	7.7(4.1)	0.6	0.9	0.5–0.6
J104223+092708	0.592	21.4(11.7)	97.9(5.7)	11.5(4.0)	31.0(17.0)	141.9(11.1)	33.3(11.7	1.4	3.5	7.3–8.0
J113108+202151	0.563	110.5(9.6)	247.3(6.8)	47.1(7.5)	141.8(12.3)	317.4(11.7)	120.8(19.1	6.3	11.8	16.5–17.7
J120538+604057	0.434	33.9(7.5)	19.1(2.5)	6.3(2.7)	23.3(5.2)	13.1(2.3)	8.7(3.7)	1.0	1.0	0.2–0.3
J120908+022734[e]	0.669	42.8(7.2)	50.1(6.1)	9.6(4.2)	83.7(14.0)	97.8(15.9)	37.4(16.5)	3.7	3.9	1.4–1.8
J121510+141802	0.421	31.2(8.2)	34.3(2.8)	7.3(2.6)	20.0(5.3)	22.0(2.4)	9.3(3.3)	0.9	1.0	0.4–0.5
J122752+165522	0.565	34.5(6.8)	43.0(4.1)	14.0(6.6)	44.6(8.8)	55.6(7.0)	36.2(17.0)	2.0	3.8	4.7–5.0
J125339+175832	0.401	19.4(4.6)	53.8(3.3)	7.7(2.7)	11.1(2.6)	30.7(2.6)	8.8(3.1)	0.5	1.0	1.2
J132542+255525	0.433	6.9(5.5)	34.6(2.9)	11.7(3.3)	4.7(3.8)	23.7(2.7)	16.0(4.6)	0.2	1.7	18.1–45.2
J142421+453523	0.421	16.4(8.0)	26.2(3.3)	11.9(4.8)	10.5(5.2)	16.8(2.8)	15.3(6.2)	0.5	1.7	5.4–7.2
J154542+505759	0.525	18.6(11.8)	75.8(5.0)	6.9(3.2)	20.1(12.8)	82.2(7.2)	14.9(7.0)	0.9	1.6	1.7–1.8
J161728+061604[e]	0.788	32.1(4.9)	34.3(9.8)	$\leq$9.5	93.3(14.3)	99.8(38.1)	$\leq$27.5	4.1	–	–
J165508+224150	0.453	11.9(4.8)	39.7(5.2)	6.5(3.5)	9.0(3.6)	30.2(5.3)	9.9(5.4)	0.4	1.1	2.3–2.6
J165632+414617	0.662	18.8(5.1)	38.5(6.9)	7.6(4.7)	35.7(9.7)	73.2(17.4)	28.9(17.7)	1.6	3.0	3.8–4.0

[a]Due to fibre losses, luminosities and SFRs should be considered as lower limits. [b]Luminosities are *not* corrected for dust extinction. [c]Updated SFR calibrations for [O II] (Kewley, Geller & Jansen 2004) and Hα (Kennicutt 1998) were taken from Argence & Lamareille (2009), assuming an intrinsic Balmer decrement of 2.85: Hα = 2.85 Hβ. [d]Self-consistent two-lines calibration ([O II]+Hβ) from Argence & Lamareille (2009). [e](Mg II+[O II])-selected galaxies.

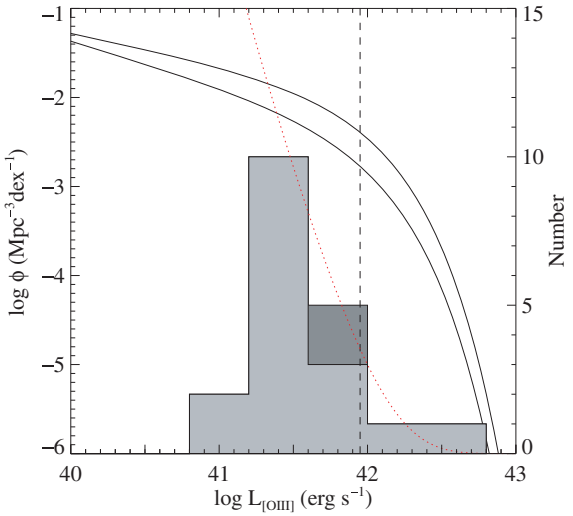

Figure 3. The distribution of [O III] luminosities for the intervening galaxies (light histogram: [O III]-selected, dark histogram: (Mg II+[O II])-selected) is compared to the [O III] luminosity functions at $z = 0.4$ (higher curve) and 0.64 (lower curve), to be read on the left axis. The vertical dashed line marks the position of $L^\star_{[O\,III]} = 8.9 \times 10^{41}$ erg s^{-1} (Hippelein et al. 2003). The dotted curve represents the [O III] luminosity function in linear space and arbitrary scaling to illustrate the completeness of the luminosity distribution of the galaxies presented in this paper.

line ratios is necessary to break the degeneracy (see Kewley & Ellison 2008). Unfortunately, the corresponding lines are not covered by the SDSS spectra. Therefore, we provide the lower and upper estimates of the metallicity derived using the R23 ratio only. The oxygen metallicity estimated using uncorrected fluxes are given in Table 3. The columns $R23_l$ and $R23_u$ refer to the lower and upper branch of R23. It is known that the value of (O/H) estimated with and without dust corrections are consistent with each other within 0.1 dex (Lamareille et al. 2006; Moustakas & Kennicutt 2006).

Table 3. Emission-line metallicities.

QSO	z_{gal}	log(O/H) + 12	
		$R23_l$	$R23_u$
J080808+064108	0.433	8.10	8.52
J081154+202148	0.445	–	–
J091417+325955	0.444	–	–
J092913+302225	0.439	8.00	8.59
J094041+341535	0.447	7.95	8.60
J095228+032616	0.419	8.22	8.45
J104223+092708	0.592	8.27	8.41
J113108+202151	0.563	8.08	8.53
J120538+604057	0.434	8.36	8.37
J120908+022734†	0.669	8.38	8.33
J121510+141802	0.421	8.33	8.37
J122752+165522	0.565	7.92	8.66
J125339+175832	0.401	8.24	8.42
J132542+255525	0.433	7.40	8.86
J142421+453523	0.421	7.59	8.83
J154542+505759	0.525	8.56	8.21
J161728+061604†	0.788	–	–
J165508+224150	0.453	8.06	8.54
J165632+414617	0.662	8.09	8.53

For comparison, the solar value is log(O/H) + 12 = 8.69 ± 0.05 (Asplund et al. 2009). No correction for dust has been applied when measuring R23. † (Mg II+[O II])-selected galaxies.

Maier et al. (2005) and Mouhcine et al. (2006) pointed out that, for the intermediate-redshift galaxies where the degeneracy is lifted using other line indicators, the (O/H) is found to be predominantly close to the value obtained for the upper branch. We find that the (O/H) range in our sample obtained using $R23_u$ compares well with that measured in intermediate-redshift field galaxies and cluster galaxies (see Kobulnicky & Phillips 2003; Kobulnicky et al. 2003; Lilly, Carollo & Stockton 2003; Mouhcine et al. 2006). This confirms that our galaxy selection is not heavily biased towards high- or low-metallicity galaxies. However, we wish to point out that the

Table 4. Absorption line measurements.

QSO	z_{gal}	Δv (km s^{-1})	$E(B-V)^a$	Rest equivalent widths (Å)				
				Fe IIλ2586	Fe IIλ2600	Mg IIλ2796	Mg IIλ2803	Mg Iλ2852
J080808+064108	0.433	4(16)	0.01	–	–	2.5(0.5)	1.9(0.4)	0.8(0.6)
J081154+202148	0.445	41(15)	0.04	–	–	1.2(0.4)	1.1(0.3)	0.3(0.3)
J091417+325955[b]	0.444	–	0.32	–	–	–	–	–
J092913+302225	0.439	−96(13)	0.02	–	–	2.3(0.8)	1.9(0.6)	1.3(0.4)
J094041+341535	0.447	−16(16)	−0.02[d]	–	–	2.1(0.6)	2.1(0.5)	0.6(0.3)
J095228+032616	0.419	50(18)	0.15	–	–	2.0(0.7)	0.6(0.2)	2.5(0.7)
J104223+092708	0.592	−105(16)	0.02	<0.6	<0.6	0.6(0.2)	0.3(0.2)	<0.25
J113108+202151	0.563	32(7)	−0.01[d]	2.4(0.4)	2.3(0.4)	4.1(0.4)	3.6(0.3)	<0.3
J120538+604057	0.434	59(21)	0.06	–	–	2.5(0.8)	1.5(0.5)	0.8(0.9)
J120908+022734[c]	0.669	11(14)	0.01	2.1(0.3)	2.7(0.3)	3.2(0.2)	3.2(0.3)	1.2(0.2)
J121510+141802	0.421	18(21)	0.09	–	–	1.6(0.8)	0.6(0.5)	0.9(0.7)
J122752+165522	0.565	71(12)	0.04	2.5(0.6)	3.9(0.6)	<12.8	<5.1	–
J125339+175832	0.401	−41(9)	0.18	–	–	1.2(0.2)	1.4(0.4)	0.2(0.3)
J132542+255525	0.433	–	0.03	–	–	<0.6	<0.6	<0.6
J142421+453523	0.421	−97(22)	0.04	–	–	3.6(0.7)	3.1(0.7)	<0.7
J154542+505759	0.525	−58(10)	−0.01[d]	1.4(0.5)	1.0(0.5)	1.2(0.3)	2.0(0.4)	0.9(0.5)
J161728+061604[c]	0.788	104(13)	0.07	2.4(0.3)	2.7(0.3)	3.1(0.2)	3.2(0.3)	1.3(0.3)
J165508+224150	0.453	−57(12)	−0.02[d]	–	–	2.2(0.3)	2.2(0.3)	0.6(0.3)
J165632+414617	0.662	28(1)	0.03	1.9(0.6)	1.8(0.6)	2.6(0.7)	2.4(0.8)	1.0(0.7)

[a]Negative values for $E(B-V)$ are the consequence of intrinsic quasar shape variations. [b]A Lyman-limit system is present at $z_{abs} \sim 4.5$ towards this quasar, preventing absorption line measurements at $\lambda < 5000$ Å. [c](Mg II+[O II])-selected galaxies.

(O/H) determination based on $R23_u$ for the Ca II and DLA-selected galaxies (Zych et al. 2007) are slightly higher than the values we find for the galaxies in our sample.

4 ANALYSIS OF ABSORPTION FEATURES

The emission-line analysis presented in the previous section clearly suggests that the distribution of physical properties of the emission-line galaxies in our sample are consistent with that found for field galaxies at similar redshift range. Thus, we have an unbiased, albeit small sample of star-forming galaxies where we will be able to probe the nature of absorption lines they produce in the spectra of background QSOs that are at an impact parameter $\leq$10 kpc.

In this section, we analyse the absorption lines produced in the QSO spectra by the emitting galaxies. For this, each quasar spectrum is normalized by *dividing* the observed spectrum by the quasar continuum. In principle, the galaxy continuum emission should be subtracted prior to normalization of the spectrum. However, continuum emission from the galaxies is expected to be very small compared to that of the QSO and should have a negligible effect on the measurement of absorption line parameters. The equivalent widths of metal absorption lines are then obtained by simultaneous Gauss-profile fitting, using a single absorption redshift (i.e. z_{abs}) to describe all detected absorption lines but allowing for it to be different from z_{gal} obtained from emission lines. The normalized spectra and Gaussian fits to the absorption lines are also shown in Fig. 2. The rest equivalent width of Fe II $\lambda\lambda$2586, 2600, Mg II $\lambda\lambda$2796, 2803 and Mg I λ2852 are provided in Table 4. This table also gives the redshift of the galaxy (z_{gal}) and the relative velocity shift between the centroids of the absorption and emission lines [$\Delta v/c = (z_{abs} - z_{gal})/(1 + z_{gal})$].

4.1 Mg II and Fe II absorption lines

We have chosen the redshift range such that the available SDSS spectrum of each QSO covers the expected wavelength range of Mg II absorption from the galaxy. In the case of the $z_{gal} = 0.444$ galaxy towards J091417+325959 ($z_{em} = 4.66$), the flux at the expected position of Mg II absorption is completely absorbed by a higher redshift Lyman-limit system. Similarly, in the case of the $z_{gal} = 0.565$ galaxy towards J122752+165522 the wavelength range of Mg II absorption is blended with the Lyman α forest absorption from high redshift. In the remaining 15 galaxies that are selected mainly through [O III] emission, we detect Mg II absorption with rest equivalent widths greater than 1 Å in 13 cases (see Fig. 2). This implies a detection rate of Mg II absorption with $W_{\lambda 2796} \geq 1$ Å to be $\sim$87 per cent. Interestingly, nine of these systems have $W_{\lambda 2796} \geq 2$ Å (see Table 4). This corresponds to $\sim$60 per cent detection rate.

The mean Mg II equivalent width of our [O III]-selected galaxy sample is $\langle W_{\lambda 2796} \rangle \sim 2.1$ Å (or $\langle W_{\lambda 2796} \rangle \sim 2.2$ Å when including the two [O II]-selected galaxies). In Fig. 4, we present the distribution of Mg II λ2796 equivalent widths from the galaxies in our sample and that obtained at $0.5 < z < 0.7$ from our automatic search in the SDSS-DR7. Comparing the distribution of Mg II equivalent widths with the exponential parametrization by Nestor, Turnshek & Rao (2005), we find that our sample of Mg II-selected absorbers is probably complete down to $W_{\lambda 2796} = 1$ Å. Since [O III]-selected Mg II absorbers are selected without any a priori information on their absorbing properties, we can compare the two distributions for equivalent widths above this value. It is clear from the figure that the Mg II equivalent widths in our [O III]-selected sample are predominantly distributed towards higher equivalent widths. A double-side KS test gives a probability 1.5×10^{-4} that the two distributions (for $W_{\lambda 2796} \geq 1$ Å) arise from the same parent population. Therefore, Mg II absorption lines associated to line-emitting galaxies are clearly characterized by larger equivalent widths than the Mg II-selected absorbers. Below, we address the question of what fraction of strong Mg II absorption systems in the same redshift range are detected in our emission-line search.

In our [O III]-emission selected sample, we cover the rest wavelength range of Fe II $\lambda\lambda$2586, 2600 for five galaxies. We detect Fe II absorption lines in all the cases when $W_{\lambda 2796} \geq 1$ Å. In all these

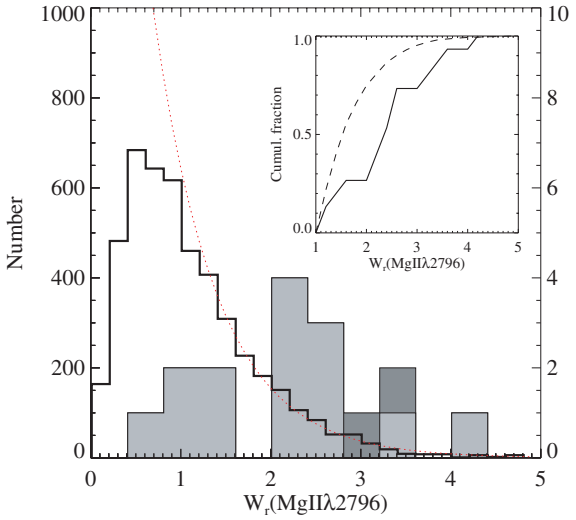

Figure 4. Distribution of Mg II λ2796 rest equivalent widths for the overall SDSS Mg II sample (with $z_{abs} = 0.5$–0.7, unfilled histogram) and that of the [O III]-selected galaxies (light grey histogram). The values for the two (Mg II+[O II])-selected galaxies are represented in dark grey. The two distributions are represented with different scales for presentation purpose only (SDSS left, galaxy sample right). The dotted line represents the parametrization by Nestor et al. (2005), scaled to match the number of systems with $W_{\lambda 2796} \geq 1$ Å. The cumulative distributions (starting at $W_{\lambda 2796} = 1$ Å) are shown in the inset figure (Mg II from SDSS: dashed; Mg II from our galaxy sample: solid).

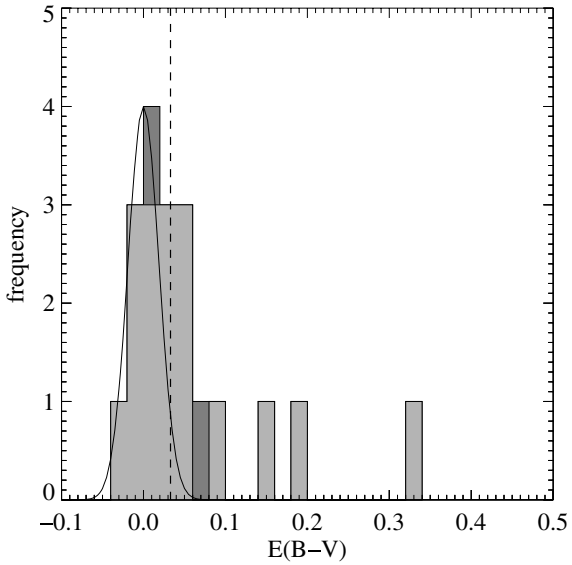

Figure 5. Distribution of $E(B-V)$ derived by fitting the SED of the background quasar. The light grey histogram represents [O III]-selected galaxies while the $E(B-V)$ values for the two (Mg II+[O II])-selected galaxies are represented in dark grey. The dashed line represents the median value for the 19 galaxies. The Gaussian illustrates the ∼0.02 mag dispersion towards negative values, presumably due to intrinsic shape variations.

cases, we find $W_{\lambda 2600} \geq 1$ Å and Mg I absorption is also detected. These systems satisfy the criteria defined by Rao, Turnshek & Nestor (2006) on the equivalent widths of Fe II, Mg II and Mg I to select damped Lyman α systems (see also Rao & Turnshek 2000). We therefore expect that more than half of the systems in our sample are bona fide DLAs with $\log N(\mathrm{H\,I}) \geq 20.3$. From fig. 3 of Steidel (1995), it is clear that galaxies associated with DLAs have low-impact parameters (i.e. ≤14 kpc) (see also Chen & Lanzetta 2003; Rao et al. 2003).

4.2 Dust extinction towards QSOs

From fig. 1 of Argence & Lamareille (2009), we can see that the average dust optical depth in star-forming galaxies in their SDSS sample is ∼1.2. This corresponds to an A_V of 1.3 and $E(B-V)$ of 0.42 for the assumed $R_V = 3.1$ as in the Galaxy. Therefore, quasar absorbers containing large amounts of dust and molecules are likely to be related to star-forming regions in the Universe (e.g. Noterdaeme et al. 2007; Srianand et al. 2008a). Indeed, Wild et al. (2007) statistically detected the nebular [O II] emission by stacking the spectra of quasars with strong Ca II absorbers, which have been proved to contain on an average larger amounts of dust than H I-selected DLAs (Wild et al. 2006; Nestor et al. 2008). While dusty absorbers are good candidates to search for the host galaxy emission lines, it is very interesting to verify whether the reciprocal is also true (i.e. whether the absorbers associated to star-forming galaxies within an impact parameter of 10 kpc are also dusty).

We aim here at deriving the selective reddening $E(B-V)$ of the background QSO produced by the absorbing galaxy. We use the same procedure as described in Srianand et al. (2008a) and Noterdaeme et al. (2009a). In short, we fit the observed spectrum with a SDSS quasar composite spectrum (Vanden Berk et al. 2001), reddened by an extinction law shifted to the redshift of the intervening galaxy. We use the Small Magellanic Cloud extinction curve given by Gordon et al. (2003), which has been shown to reproduce well the average reddening due to Mg II absorbers (e.g. Khare et al. 2005; Ménard et al. 2005; Wild, Hewett & Pettini 2006; York et al. 2006, see however Srianand et al. 2008a for individual cases). Other extinction laws (Large Magellanic Cloud, Milky Way) provide similar results as they are very similar in the rest wavelength range of the absorbers covered by the SDSS spectra. QSO-to-QSO intrinsic shape variations are actually the main source of uncertainties. The distribution of $E(B-V)$ is shown in Fig. 5. As can be seen from this figure, the range in intrinsic QSO ultraviolet slopes introduces a scatter of about 0.02 mag in the distribution of measured $E(B-V)$.

We found three systems (towards J091417+325955, J095228+032616 and J125339+175832) with $E(B-V) \geq 0.15$. For the first system, the reddening of the quasar is derived using a limited wavelength range because of the presence of a Lyman-limit system. The quasar also has a high redshift ($z_{QSO} = 4.66$). Therefore, the quoted value of $E(B-V)$ is unreliable. Interestingly, in the case of J095228+032616 in addition to the Mg II absorption associated with the [O III] emitting galaxy at $z_{gal} = 0.419$ there is a strong Mg II system at $z_{abs} = 0.977$ with rest equivalent width of the Mg II doublets 2.6 and 2.3 Å , respectively. This system also has very strong Fe II lines. The QSO SED is reasonably well reproduced assuming the reddening is produced in this system. However, the best-fitting curve underpredicts the flux in the blue end of the spectrum. Thus, the $E(B-V)$ value for the galaxy at $z_{gal} = 0.419$ should be considered as an upper limit. In the case of J125339+175832, the QSO appears to be very red. We also note that high-order Balmer lines as well as Ca II H and K lines are seen in absorption at the redshift of the QSO. Thus, the reddening could be mainly due to the QSO host galaxy.

As can be seen in Fig. 5, the distribution is concentrated around a median value $E(B-V) = 0.03$. Even in the top three cases with high $E(B-V)$ there are indications that the QSO colours are not necessarily reddened by the emission-line galaxy alone. The median

value is similar to or slightly higher than what is found for DLAs [$E(B-V) < 0.02$ – Murphy & Liske 2004; $E(B-V) < 0.04$ – Ellison, Hall & Lira 2005] and lower than the $E(B-V)$ found in Ca II absorbers (Wild et al. 2006) and dusty 21-cm and CO absorbers at intermediate redshifts (Srianand et al. 2008a; Noterdaeme et al. 2009a). As expected, the measured $E(B-V)$ along the QSO line of sight is much less than that measured for the SDSS galaxies using emission-line ratios (Argence & Lamareille 2009).

4.3 Relationship between emission and absorption

Ledoux et al. (2006) have established a correlation between the velocity width of low ionization lines and the metallicity of high-redshift DLAs. The slope of this relationship is shown to be consistent with the mass–metallicity relation found in local galaxies (Tremonti et al. 2004). In this section, we explore various possible correlations between star formation indicators and metallicity indicators from the emission-line fluxes and Mg II equivalent width. We make the assumption that the Mg II equivalent width reflects the number of components and the velocity spread between them and is not due to line saturation. This assumption allows us to use $W_{\lambda 2796}$ as an indicator of the velocity spread along the QSO line of sight (see e.g. Nestor et al. 2003; Ellison 2006).

In the three upper panels of Fig. 6, we plot the luminosities of [O II], Hβ and the derived SFRs as a function of the rest equivalent width of the Mg IIλ2796 line. No statistically significant correlation is seen between [O II], Hβ luminosity and $W_{\lambda 2796}$. We also do not find any strong correlation between the SFR given in the last column of Table 2 and $W_{\lambda 2796}$. However, the largest equivalent width systems are also associated to the largest luminosities. Except for the system towards J132542+255525, this is also true for the SFR. We remind that since the measured [O II] and Hβ emission-line fluxes are very low in this galaxy, it is well possible that the SFR and metallicities, which depend on the line ratios, are significantly overestimated (see Section 3.2).

In the bottom panel of Fig. 6, we plot the upper branch ($R23_u$) estimate of (O/H) as a function of $W_{\lambda 2796}$. As pointed out before, in the absence of additional constraints we end up with two degenerate metallicity measurements using R23. However, in the five line-emitting galaxies studied by Zych et al. (2007) – with similar properties as those presented here – the upper branch of R23 is preferred. A trend for increasing emission-line metallicities with increasing equivalent width can be seen. The correlation [$\log(\mathrm{O/H}) + 12 = 0.1 W_{\lambda 2796} + 8.27$] is significant at the 2σ level. However, to draw a firm conclusion on the velocity metallicity correlation we need to remove the degeneracy in the (O/H) estimation and get the velocity spread in the absorbing gas using high-resolution spectroscopy. Interestingly, a similar trend is also observed between the Mg II equivalent width and the gas-phase metallicity measured along the quasar line of sight (e.g. Nestor et al. 2003; Murphy et al. 2007).

The velocity shifts (Δv) between the emission and the absorption lines are quite small (see Table 4), at most about 100 km s^{-1}. These are consistent with the expected circular velocities of typical galaxies suggesting the absorbing gas is bounded to the emission-line galaxy. We note that the Δv we measure here are lower than that measured with respect to luminous galaxies at larger impact parameters (100–200 km s^{-1} for impact parameters ∼14–75 h^{-1} kpc; Steidel et al. 2002). In Fig. 7, we plot Δv against $W_{\lambda 2796}$. We do not find any trend between the two quantities. Although the sample is too small to conclude, this may be explained by the variety of galaxy morphologies found to be associated with low-redshift Mg II systems (Le Brun et al. 1997).

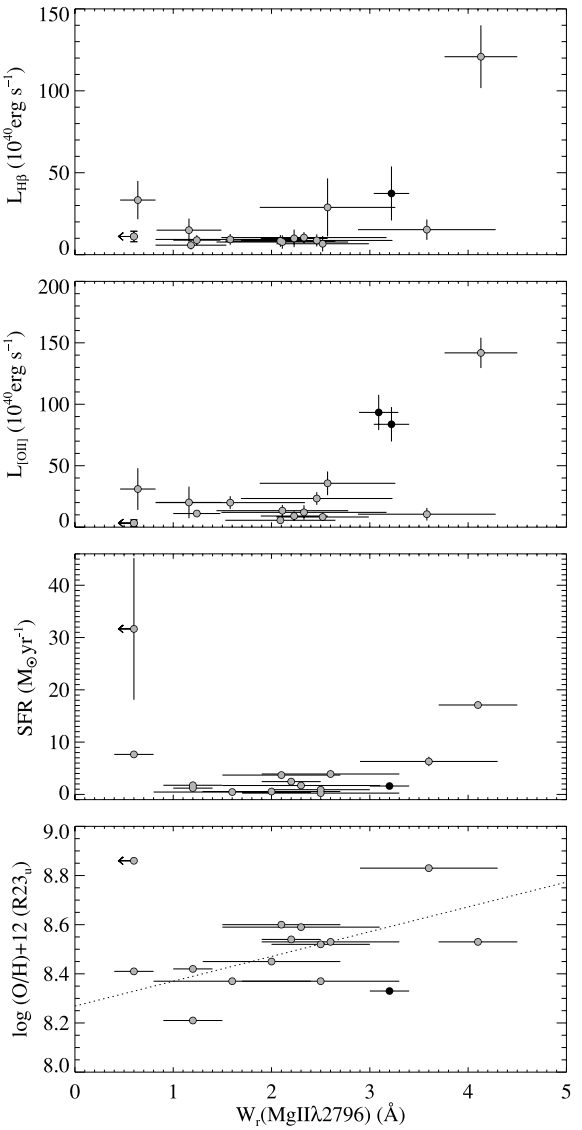

Figure 6. From top to bottom: [O II] luminosities, Hβ luminosities, SFRs and emission-line metallicities versus the Mg II equivalent width of the associated absorbing gas. The SFRs are that from the two lines calibration (last column of Table 2). The dotted line on the bottom panel represents the linear regression fit to the metallicity–equivalent width correlation. Grey circles represent [O III]-selected galaxies with black circles the (Mg II+[O II])-selected galaxies.

5 AVERAGE LINE EMISSION FROM MG II ABSORBERS

Based on our automatic search for Mg II absorption in SDSS-DR7, we find 2319, 1807, 494 and 118 systems, respectively, with $W_{\lambda 2796} \leq 1$, 1–2, 2–3 and ≥ 3 Å in the redshift range $0.5 \leq z \leq 0.7$. It is clear from the previous discussion that while most of the emission-line galaxies produce strong Mg II absorption, not all the strong Mg II absorption systems are detected in our [O III] emission searches. Indeed, the number of strong Mg II systems (with $W_{\lambda 2796} \geq 2$ Å) associated with [O III]-emitting galaxies detected within the SDSS fibre is about a hundred times less than the total

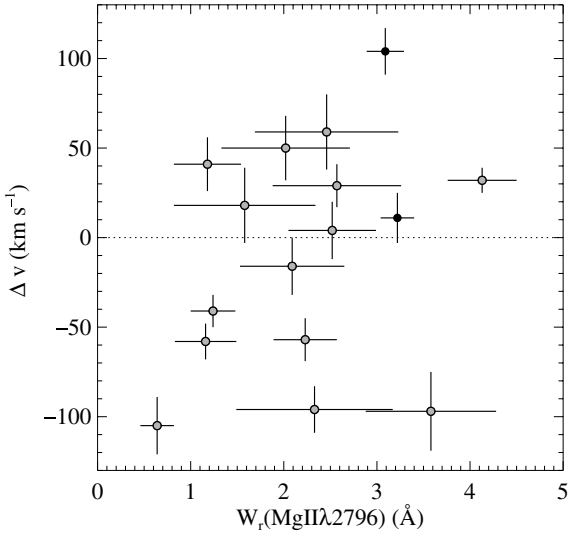

Figure 7. The velocity offset between the absorption and emission-line redshifts is plotted against the Mg II rest equivalent width. Symbols are as per Fig. 6.

number of strong Mg II absorbers. This could be due to (i) poor S/N of the spectra and/or the relative brightness between the QSO and the galaxy, (ii) low SFR in the underlying galaxies or (iii) the impact parameter of the emission-line regions being larger than ∼10 kpc (or angular separations more than 1.5 arcsec).

To explore the effect of spectral S/N and galaxy–QSO contrast further, we plot the *i*-band magnitude versus the S/N for all QSOs with intervening Mg II systems with $W_{\lambda 2796} \geq 2$ Å in the redshift range $0.5 \leq z \leq 0.7$ in Fig. 8. It is clear from the figure that most of

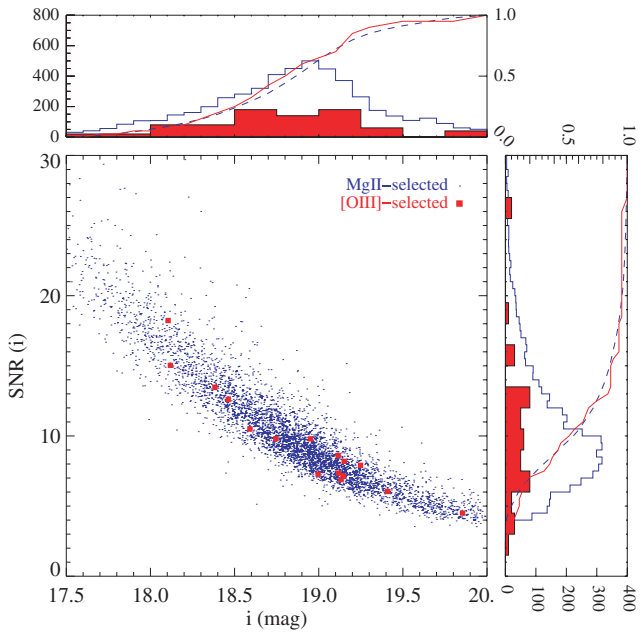

Figure 8. *i*-band S/N and magnitudes for quasars with strong ($W_{\lambda 2796} > 2$ Å) intervening Mg II-systems (black dots) and intervening [O III] emission lines (red squares). The top and right-hand panels show the distributions and cumulative distributions of magnitudes and S/N, respectively. Red filled histograms (solid lines) stand for quasars with intervening [O III]-emission lines while blue unfilled histograms (dashed line) stand for quasars selected for strong intervening Mg II absorption lines.

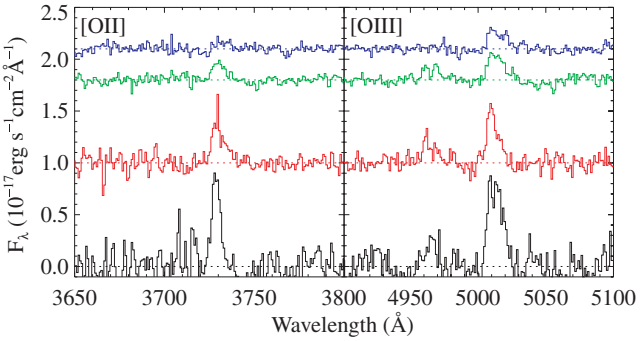

Figure 9. [O II] (left) and [O III] (right) emission lines from stacking QSO spectra with intervening Mg II absorbers at $0.5 < z_{\rm abs} < 0.7$ with different Mg II λ2796 rest equivalent widths. From top to bottom: $W_{\lambda 2796} < 1$; $1 \leq W_{\lambda 2796} < 2$; $2 \leq W_{\lambda 2796} < 3$; $W_{\lambda 2796} \geq 3$ Å. The continuum-substracted spectra are shifted by a constant for display purpose.

these QSOs have *i*-band magnitudes in a narrow range 18–19.5 mag. The spectral S/N is constant within a factor of 2 in this magnitude range. To the eye, there seems to be a tendency for the [O III]-selected galaxies to prefer slightly fainter *i*-band magnitude (see the upper histogram). However, KS tests do not indicate the differences between two populations to be statistically significant. Thus, it seems that there is no clear indication that we could have missed strong emission from most of the Mg II systems mainly because of the poor S/N. It is also clear from Fig. 1 that, in the *i* magnitude range 18–20 mag, the spectral S/N achieved in all the QSO spectra are good enough to detect emission lines with peak flux in excess of 10^{-17} erg s^{-1} cm^{-2} Å^{-1}. Thus, the lack of direct detection of emission lines from the strong Mg II systems is consistent with either their fluxes being small or the impact parameters being large enough so that the emitting regions are not falling inside the fibre.

In order to investigate the *average* [O II] and [O III] emission within 1.5 arcsec of associated intervening Mg II absorption systems, we build several composite spectra corresponding to different ranges of Mg II equivalent widths. The quasar spectra featuring Mg II absorption lines in the range $z_{\rm abs} = 0.5$–0.7 were shifted to the absorbers rest frame and combined together using an arithmetic mean. Note that our direct detections are not included in the stacking. The continuum flux in the vicinity of the emission lines was removed using a second-order polynomial fit. Fig. 9 present the resulting composite [O II] and [O III] emission lines from intervening Mg II absorption systems with rest equivalent width $W_{\lambda 2796}$ in the ranges ≤1, 1–2, 2–3 and >3 Å. From this figure, it is clear that the strength of the emission lines increases with the Mg II equivalent widths. This can also be seen from Table 5 where we give the average luminosity of [O II] and [O III] emission lines for different subsamples defined using $W_{\lambda 2796}$. We note that the average [O II] flux for $W_{\lambda 2796}$ ∼ 1–2 Å is similar to that obtained by Wild et al. (2007) for Mg II-selected DLAs ($1 < W_{\lambda 2796}/W_{\lambda 2600} < 2$ and $W_{\lambda 2796} > 0.6$; see Rao et al. 2006).

Table 5. Luminosities of the emission lines in the stacked spectrum.

Line	Average luminosity[a] for systems with			
	$W < 1$Å	$1 < W < 2$ Å	$2 < W < 3$ Å	$W > 3$ Å
[O II]	0.5(0.2)	1.4(0.1)	3.2(0.2)	5.1(0.6)
[O III]	2.5(0.3)	3.5(0.3)	5.1(0.4)	10.0(0.9)

[a]In units of 10^{40} erg s^{-1}.

The average [O III] luminosity found by stacking Mg II systems with $W_{\lambda 2796} > 2$ Å is roughly $L^{\star}_{[\mathrm{O\,III}]}/10$ and close to the lowest luminosity we directly measure in the [O III]-selected galaxies (in $z_{\mathrm{gal}} = 0.444$ towards J091417+325955). Note that in this case the detection is enabled by the low QSO flux ($i = 19.5$ mag). As discussed in Section 2.1, this system would not have been detected had the QSO being brighter. Zych et al. (2007) have detected emission lines at the redshift of the Ca II absorber towards J224630.62+131048.5. The rest equivalent width of Mg IIλ2796 is 2.2 Å. No clear emission lines are detected in the SDSS spectrum. However, a galaxy is clearly seen within the area covered by the fibre (See fig. 5 of Zych et al. 2007) and emission lines (with integrated [O III] flux of 8×10^{-17} erg s^{-1} cm^{-2} i.e. lower than our detection limit with SDSS) are detected in the Very Large Telescope/Focal Reducer and low dispersion Spectrograph (FORS) spectra. We also note that the [O III] luminosity of this galaxy is similar to the stacked luminosity obtained using systems with $2 < W_{\lambda 2796} < 3$ Å.

Direct observations of field galaxies at $z \sim 0.6$ show that the sizes of star-forming galaxies are typically less than 10 kpc (Lilly et al. 2003; de Mello et al. 2006; Dahlen et al. 2007). Integral field spectroscopic observations of Mg II absorbers at $0.8 < z < 1.2$ by Bouché et al. (2007) also confirms that Hα-emitting regions of Mg II-selected galaxies have similar sizes. This means that the galaxies contributing to the stacked emission lines should have impact parameters less than about 20 kpc. Therefore, it is most unlikely that a bright galaxy at high-impact parameter (several tens of kpc) will contribute to the average detection of emission lines in the stacked spectrum. The stacking method alone does not provide the higher moments of the $L_{[\mathrm{O\,III}]}$ distribution. However, with additional constraints on the galaxy sizes and the small number of direct detections, our results are consistent with at least part of the strong Mg II absorbers arising from low $L_{[\mathrm{O\,III}]}$ luminosity galaxies at low-impact parameters, as seen in the case of J224630+131048 (Zych et al. 2007).

It is also interesting to see that the [O III] and [O II] emission lines are detected in the stacked spectrum even when we consider only low equivalent widths. In particular, there are roughly four times more systems with $1 \leq W_{\lambda 2796} \leq 2$ Å compared to that with $2 \leq W_{\lambda 2796} \leq 3$ Å. However, the average [O III] and [O II] luminosities are less only by a factor of 2. Even though our Mg II-selected systems with low rest equivalent widths ($W_{\lambda 2796} < 1$ Å) are likely to be biased towards QSOs with high S/N spectra, it is interesting to see that we detect [O II] emission at 3σ level and that [O III] is detected at $>5\sigma$. This means that galaxies with low-impact parameters can also produce low equivalent width absorption lines. This is consistent with the fact that we do not detect Mg II absorption with $W_{\lambda 2796} \geq 1$ Å in two of our [O III]-selected galaxies.

In summary, star-forming galaxies with low [O III] luminosities seem to provide an important contribution to the population of Mg II absorption selected galaxies.

6 THE CASE OF SDSS J113108+202151

In this section, we study the galaxy at $z_{\mathrm{gal}} = 0.563$ towards J113108+202151 which presents the strongest emission lines in our $z > 0.4$ sample and also the strongest associated Mg II absorption lines. An extended galaxy (SDSS J113108.31+202147.3) is clearly visible close to the quasar line of sight in the SDSS image, with its centroid located at about 3.5 arcsec from the quasar image and extended towards the quasar image (see Fig. 10). Moreover, the photometric redshift provided by SDSS, $z = 0.65 \pm 0.07$, is close to that of the detected emission and absorption lines. This is therefore a very good case to study the connection between the galaxy and the absorber.

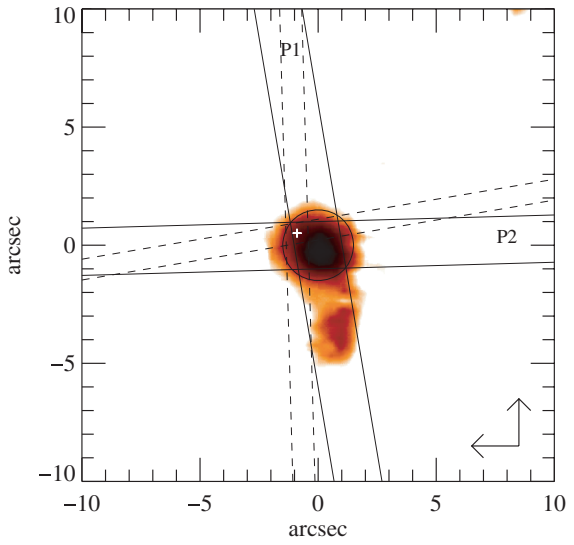

Figure 10. Layout of the slits (solid lines) and SDSS fibre (circle) on the quasar SDSS J113108+202151. The positions (P1 and P2) are indicated on top (as represented in Fig. 11) of the slits. The dashed lines represent the 1σ constraints on the centroid of the intervening emission-line galaxy, as obtained from each slit orientation. The cross marks the centroid of the galaxy.

In order to obtain an accurate measurement of the location of the emission region, we performed long-slit spectroscopy with the 2-m telescope of the IGO. Observations were carried out on 2009 March 20 using IUCAA Faint Object Spectrograph and Camera. A 2-arcsec slit and GR7 grism covering the wavelength range between 3900 and 6800 Å were used. The detector used is a LN2 cooled thinned 2k × 2k CCD camera. Each pixel on the CCD covers 0.34 arcsec of sky which corresponds to 1.4 Å using the above grism. Three exposures of 2700 s each were taken at slit position 10° from North (P1) and two exposures of 2700 s each were taken at slit position 92° from North (P2). The slit positions have been indicated in Fig. 10. For flat fielding halogen lamp flats were used. Helium and neon lamps were used simultaneously for getting comparison spectrum. The IRAF routine RESPONSE was used for making a normalized flat. The DOSLIT package has been used to extract and calibrate the 1D spectrum. Two-dimensional (2D) analysis was performed using the method described in Vivek et al. (2009).

Fig. 11 represents the 2D spectra obtained with the two-slit orientations as illustrated in Fig. 10. We removed the quasar trace by fitting a Gaussian in the spatial direction, whose amplitude is allowed to vary smoothly (second-order polynomial) with the wavelength. We also left the position of the Gaussian in the spatial direction to vary linearly with the wavelength, to take into account the possible misalignment between the quasar trace and the pixels of the CCD.

The [O II] emission can be seen as a bright spot in both spectra. Interestingly, despite aligning the slit with the galaxy seen at 3.5 arcsec from the quasar (see Fig. 10), there is no emission line at the corresponding position (marked by an 'X') in the 2D spectrum. On the contrary, while the second slit angle was chosen to avoid including the galaxy, the [O II] emission is still detected. This demonstrates the galaxy seen on the SDSS image is not responsible for the detected emission lines. Interestingly, this galaxy does not produce any other detectable absorption line system in the QSO spectra over the wavelength range covered by the SDSS and IGO

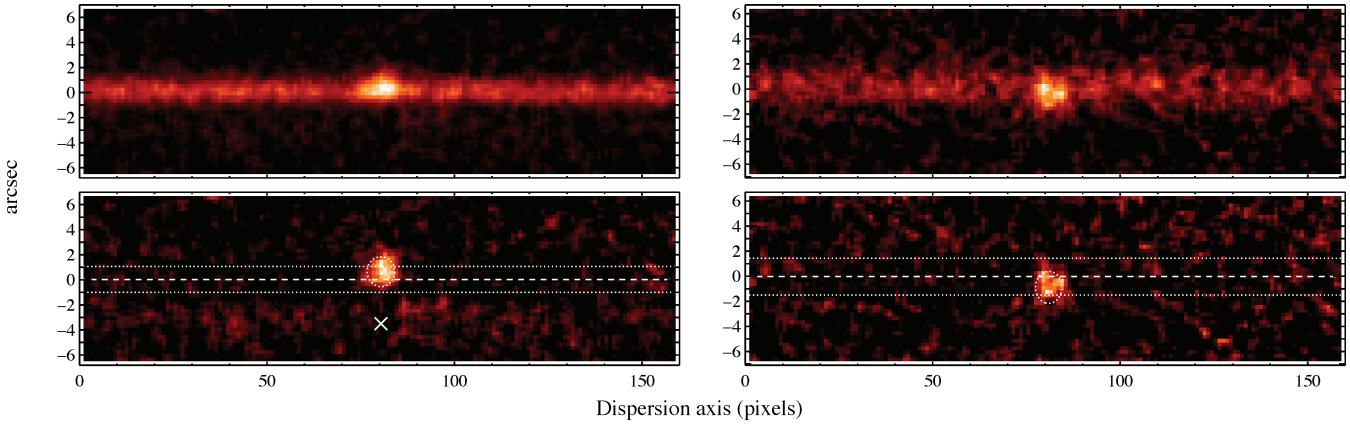

Figure 11. The background-subtracted 2D spectra of the quasar SDSS J113108+202151 and the galaxy at $z_{\rm gal} = 0.56$. Top: total (quasar+galaxy) spectra obtained with two-slit orientations (left: P1, 10° from North; right: P2, 92° from North, see Fig. 10). Bottom: same spectra after removing the quasar trace. The centre of the quasar trace is represented by the horizontal dashed lines, and its FWHM by the horizontal dotted lines. The ellipses represent the FWHM of a 2D Gaussian fitted over the galaxy emission line. The 'X' on the bottom-left panel represent the expected position of a [O II] emission line located 3.5 arcsec south from the quasar, i.e. at the centroid of the galaxy resolved by the SDSS. The data have been smoothed 2 × 2 pixels.

spectra. We obtained the centroid of the [O II] emission by fitting the line with a 2D Gaussian function. From triangulating the positions with the two slits, we are able to put a good constraint on the position of the emitting region. We measure an impact parameter $D = 1.1$ arcsec, which corresponds to 7 kpc at the redshift of the galaxy. The centroid of the emission region is shown as a white cross on Fig. 10. We see the integrated [O II] flux measured in IGO and SDSS spectra are consistent with one another suggesting that the whole line-emitting region is within the SDSS fibre.

7 SUMMARY AND DISCUSSION

Taking advantage of the available ∼100 000 fibre spectra of quasars in the SDSS II DR7, we build a unique sample of 46 star-forming galaxies at $z < 0.8$ detected through their nebular ([O III] and/or [O II]) emission lines seen on top of the background quasar spectra. We show the detectability of [O III] lines is not biased by the luminosity of the background quasars.

We study both the emission and absorption properties of a subsample of 17 galaxies at $z \geq 0.4$ for which the expected positions of Mg II lines are covered by the SDSS spectra. The detections show that we are probing an unbiased population of low-luminosity [O III]-emitting galaxies at small impact parameters ($\lesssim$10 kpc; i.e. the SDSS fibre radius) from the quasar lines of sight. We find that typical properties (metallicity, SFRs, kinematics) of these galaxies are similar to that of normal star-forming galaxies at these redshifts. The low $E(B - V)$ we measure along the quasar lines of sight indicates that the absorption lines arise from regions relatively free of dust. This implies that quasar absorbers selected upon the presence of cold gas and dust features (Srianand et al. 2008a,b; Noterdaeme et al. 2009a) might still be the best way to probe the interstellar medium in the densest regions of normal galaxies in the distant Universe.

We find that the equivalent widths of Mg II absorption lines arising from the [O III]-selected galaxies are skewed towards higher equivalent widths than the overall population of Mg II absorbers. However, the [O III]-selected Mg II absorbers represent only a small fraction of the overall Mg II population. From stacking the spectra of quasars featuring strong Mg II absorbers, we detect the [O II] and [O III] emission lines. The average line fluxes are below our typical detection limit in individual spectrum. This suggests that at least part of the strong ($W_{\lambda 2796} > 1$ Å) Mg II absorption systems arise from low-luminosity galaxies at small impact parameters. Also strong Mg II systems have been detected at higher rate around clusters (Lopez et al. 2008). In such cases, the halo sizes of Mg II systems are inferred to be less than $10\,h^{-1}$ kpc (Padilla et al. 2009).

The absorption properties of the galaxies indicate that at least half of the emission-line galaxies in our sample, if not all, contain sufficient neutral gas to produce damped Lyman α absorption (Rao et al. 2006) as well as 21-cm absorption Gupta et al. (2009) along the quasar line of sight. Unfortunately, most of the QSOs in our sample do not have sufficient radio fluxes to carry out 21-cm searches.

SDSS spectra allowed us to explore the possible connections between various parameters of the galaxies (such as metallicity, dust content and kinematics) derived from the absorbing gas and that derived from emission lines in a limited redshift range. Nevertheless, our representative sample of 46 galaxies presented in Table 1 is ideally suited for several follow-up observations using space- and ground-based telescopes. This should allow one to explore various issues such as the connection between the reddening along the QSO line of sight and the dust extinction in the line-emitting region, the comparison between the emission and absorption line metallicities, the dependence of the properties of the absorbing gas on the galaxy morphology, kinematics and impact parameter, etc. Finally, we perform long-slit observations of the most luminous galaxy with Mg II absorption in our sample (SDSS J113108+202151). We show that the [O II] emission detected in the SDSS spectrum is not detected in the extended bright galaxy seen on the SDSS image. This once again suggests that one should be cautious in associating intervening absorption (or emission) to bright galaxies seen in the field with photometric redshift measurements only.

ACKNOWLEDGMENTS

We gratefully thank the anonymous referee for thorough reading of the paper and helpful comments and suggestions. We also thank P. Petitjean and P. Boissé for useful comments on the manuscript. PN acknowledges support from the French Ministry of Foreign and European Affairs. We wish to acknowledge the IUCAA/IGO staff for their support during our observations. We acknowledge the use of the SDSS. Funding for the SDSS and SDSS-II has been provided by the Alfred P. Sloan Foundation, the Participating

Institutions, the National Science Foundation, the U.S. Department of Energy, the National Aeronautics and Space Administration, the Japanese Monbukagakusho, the Max Planck Society and the Higher Education Funding Council for England. The SDSS Web Site is http://www.sdss.org. The SDSS is managed by the Astrophysical Research Consortium for the Participating Institutions. The Participating Institutions are the American Museum of Natural History, Astrophysical Institute Potsdam, University of Basel, University of Cambridge, Case Western Reserve University, University of Chicago, Drexel University, Fermilab, the Institute for Advanced Study, the Japan Participation Group, Johns Hopkins University, the Joint Institute for Nuclear Astrophysics, the Kavli Institute for Particle Astrophysics and Cosmology, the Korean Scientist Group, the Chinese Academy of Sciences (LAMOST), Los Alamos National Laboratory, the Max-Planck-Institute for Astronomy (MPIA), the Max-Planck-Institute for Astrophysics (MPA), New Mexico State University, Ohio State University, University of Pittsburgh, University of Portsmouth, Princeton University, the United States Naval Observatory and the University of Washington.

REFERENCES

Argence B., Lamareille F., 2009, A&A, 495, 759
Asplund M., Grevesse N., Sauval A. J., Scott P., 2009, ARA&A, 47, 481
Bechtold J., Ellingson E., 1992, ApJ, 396, 20
Bergeron J., Boissé P., 1991, A&A, 243, 344
Bouché N., Lehnert M. D., Aguirre A., Péroux C., Bergeron J., 2007, MNRAS, 378, 525
Bowen D. V., Blades J. C., Pettini M., 1995, ApJ, 448, 634
Chen H., Lanzetta K. M., 2003, ApJ, 597, 706
Christensen L., Noterdaeme P., Petitjean P., Ledoux C., Fynbo J. P. U., 2009, A&A, 505, 1007
Dahlen T., Mobasher B., Dickinson M., Ferguson H. C., Giavalisco M., Kretchmer C., Ravindranath S., 2007, ApJ, 654, 172
de Mello D. F., Wadadekar Y., Dahlen T., Casertano S., Gardner J. P., 2006, AJ, 131, 216
Ellison S. L., 2006, MNRAS, 368, 335
Ellison S. L., Hall P. B., Lira P., 2005, AJ, 130, 1345
Gordon K. D., Clayton G. C., Misselt K. A., Landolt A. U., Wolff M. J., 2003, ApJ, 594, 279
Gupta N., Srianand R., Petitjean P., Noterdaeme P., Saikia D. J., 2009, MNRAS, 398, 201
Hippelein H. et al., 2003, A&A, 402, 65
Kacprzak G. G., Churchill C. W., Steidel C. C., Murphy M. T., 2008, AJ, 135, 922
Kennicutt R. C. Jr., 1998, ARA&A, 36, 189
Kewley L. J., Ellison S. L., 2008, ApJ, 681, 1183
Kewley L. J., Geller M. J., Jansen R. A., 2004, AJ, 127, 2002
Khare P. et al., 2005, in Williams P., Shu C.-G., Menard B., eds, IAU Colloq. 199, Probing Galaxies through Quasar Absorption Lines. Cambridge Univ. Press, Cambridge, p. 427
Kisielius R., Storey P. J., Ferland G. J., Keenan F. P., 2009, MNRAS, 397, 903
Kobulnicky H. A., Phillips A. C., 2003, ApJ, 599, 1031
Kobulnicky H. A., Kennicutt R. C. Jr, Pizagno J. L., 1999, ApJ, 514, 544
Kobulnicky H. A. et al., 2003, ApJ, 599, 1006
Lamareille F., Contini T., Brinchmann J., Le Borgne J.-F., Charlot S., Richard J., 2006, A&A, 448, 907
Le Brun V., Bergeron J., Boisse P., Deharveng J. M., 1997, A&A, 321, 733
Ledoux C., Petitjean P., Fynbo J. P. U., Møller P., Srianand R., 2006, A&A, 457, 71
Lilly S. J., Carollo C. M., Stockton A. N., 2003, ApJ, 597, 730
Lopez S. et al., 2008, ApJ, 679, 1144
Ly C. et al., 2007, ApJ, 657, 738
Maier C., Lilly S. J., Carollo C. M., Stockton A., Brodwin M., 2005, ApJ, 634, 849
Markwardt C. B., 2009, preprint (arXiv:0902.2850)
Ménard B., Zibetti S., Nestor D., Turnshek D., 2005, in Williams P., Shu C.-G., Menard B., eds, IAU Colloq. 199, Probing Galaxies through Quasar Absorption Lines. Cambridge Univ. Press, Cambridge, p. 86
Mouhcine M., Bamford S. P., Aragón-Salamanca A., Nakamura O., Milvang-Jensen B., 2006, MNRAS, 369, 891
Moustakas J., Kennicutt R. C. Jr., 2006, ApJ, 651, 155
Murphy M. T., Liske J., 2004, MNRAS, 354, L31
Murphy M. T., Curran S. J., Webb J. K., Ménager H., Zych B. J., 2007, MNRAS, 376, 673
Nestor D. B., Rao S. M., Turnshek D. A., Vanden Berk D., 2003, ApJ, 595, L5
Nestor D. B., Turnshek D. A., Rao S. M., 2005, ApJ, 628, 637
Nestor D. B., Pettini M., Hewett P. C., Rao S., Wild V., 2008, MNRAS, 390, 1670
Noterdaeme P., Petitjean P., Srianand R., Ledoux C., Le Petit F., 2007, A&A, 469, 425
Noterdaeme P., Ledoux C., Srianand R., Petitjean P., Lopez S., 2009a, A&A, 503, 765
Noterdaeme P., Petitjean P., Ledoux C., Srianand R., 2009b, A&A, 505, 1087
Padilla N., Lacerna I., Lopez S., Barrientos L. F., Lira P., Andrews H., Tejos N., 2009, MNRAS, 395, 1135
Rao S. M., Turnshek D. A., 2000, ApJS, 130, 1
Rao S. M., Nestor D. B., Turnshek D. A., Lane W. M., Monier E. M., Bergeron J., 2003, ApJ, 595, 94
Rao S. M., Turnshek D. A., Nestor D. B., 2006, ApJ, 636, 610
Spergel D. N. et al., 2003, ApJS, 148, 175
Srianand R., Gupta N., Petitjean P., Noterdaeme P., Saikia D. J., 2008a, MNRAS, 391, L69
Srianand R., Noterdaeme P., Ledoux C., Petitjean P., 2008b, A&A, 482, L39
Steidel C. C., 1995, in Meylan G., ed., QSO Absorption Lines. Springer, Berlin, p. 139
Steidel C. C., Kollmeier J. A., Shapley A. E., Churchill C. W., Dickinson M., Pettini M., 2002, ApJ, 570, 526
Storey P. J., Zeippen C. J., 2000, MNRAS, 312, 813
Tremonti C. A. et al., 2004, ApJ, 613, 898
Tripp T. M., Bowen D. V., 2005, in Williams P., Shu C.-G., Menard B., eds, IAU Colloq. 199, Probing Galaxies through Quasar Absorption Lines. Cambridge Univ. Press, Cambridge, p. 5
Vanden Berk D. E. et al., 2001, AJ, 122, 549
Vivek M., Srianand R., Noterdaeme P., Mohan V., Kuriakosde V. C., 2009, MNRAS, 400, L6
Wild V., Hewett P. C., Pettini M., 2006, MNRAS, 367, 211
Wild V., Hewett P. C., Pettini M., 2007, MNRAS, 374, 292
York D. G. et al., 2006, MNRAS, 367, 945
Zych B. J., Murphy M. T., Pettini M., Hewett P. C., Ryan-Weber E. V., Ellison S. L., 2007, MNRAS, 379, 1409

This paper has been typeset from a TEX/LATEX file prepared by the author.